Proceedings of ASME Turbo Expo 2011: Power for Land, Sea and Air
ASME 2011
June 6-10, 2011, Vancouver, Canada

GT2011-45969

A QUANTITATIVE COMPARISON BETWEEN A LOW ORDER MODEL AND A 3D FEM CODE FOR THE STUDY OF THERMOACOUSTIC COMBUSTION INSTABILITIES

Giovanni Campa*
Sergio Mario Camporeale
D.I.M.eG.
Politecnico di Bari
via Re David 200, 70125 Bari, Italy
Email: g.campa@poliba.it

Anaïs Guaus
Julien Favier
Matteo Bargiacchi
Alessandro Bottaro
D.I.C.A.T.
Università di Genova
via Montallegro 1, 16145 Genoa, Italy

Ezio Cosatto
Giulio Mori
Ansaldo Energia
corso F. Perrone 118, 16161 Genoa, Italy

ABSTRACT

The study of thermoacoustic combustion instabilities has an important role for safety operation in modern gas turbines equipped with lean premixed dry low emission combustion systems. Gas turbine manufacturers often adopt simulation tools based on low order models for predicting the phenomenon of humming. These simulation codes provide fast responses and good physical insight, but only one-dimensional or two-dimensional simplified schemes can be generally examined. Large Eddy Simulation (LES) techniques are proposed in order to investigate the instability phenomenon, matching pressure fluctuations with turbulent combustion phenomena to study thermoacoustic combustion oscillations, even if they require large numerical resources. The finite element method can overcome such limitations, because it allows to examine three-dimensional geometries and to search the complex eigenfrequencies of the system.

The finite element approach solves numerically the differential equation problem converted in a complex eigenvalue problem in the frequency domain. Complex eigenvalues of the system allow us to identify the complex eigenfrequencies of the combustion system analyzed, so that we can have a valid indication of the frequencies at which thermoacoustic instabilities are expected and of the growth rate of the pressure oscillations at the onset of instability. Through the collaboration among Ansaldo Energia, Genoa University and Polytechnic University of Bari, a quantitative comparison between a low order model, called LOMTI, and the three-dimensional finite element method has been created, in order to exploit the advantages of both the methodologies.

NOMENCLATURE

A cross sectional area
c speed of sound
c_p specific heat at constant pressure
f frequency of oscillation
g growth rate
H enthalpy
J_n Bessel function of the first kind of order n
i imaginary unit
$\Im$ imaginary part
k acoustic wave number
L length
LHV Lower Heating Value
$\dot{m}$ mass flow rate
M Mach number
MM Molecular Mass
N_b number of burners
p pressure
q volumetric heat release rate
Q rate of heat release per unit area

*Address all correspondence to this author.

R gas constant
R_i radius of duct i
RR Rate of Reaction
$\Re$ real part
t time
T temperature
$\mathbf{u}$ velocity vector
u axial velocity
v radial velocity
w azimuthal velocity
$\mathbf{x}$ position vector
Y_n Bessel function of the second kind of order n

α area ratio
γ ratio of specific heats
δ thickness of duct i
ζ pressure loss coefficient
κ interaction number
λ eigenvalue $= -i\omega$
$\chi_{n,m}$ m^{th} solution of the Bessel function of order n
ρ density
τ time delay
ω angular frequency

$\bar{}$ mean quantity
$'$ fluctuating quantity
$\hat{}$ complex quantity

d downstream
eff effective
i generic section
u upstream

INTRODUCTION

Modern gas turbines for power generation are generally equipped by lean-premixed (LP) combustion technology burners in order to satisfy the strict regulations for pollutant emissions. LP combustion systems are often affected by combustion instabilities that emerge as a problem to be avoided since they may generate structural vibrations able to lead to failure of the system in the worst case.

Thermoacoustic combustion instability is a very complex issue and, over the years, several different approaches have been developed to model as well as possible this phenomenon. The methods adopted can be grouped into three different categories: low order models [1–3], LES codes [4, 5] and FEM approaches [6–8]. In low order models the whole combustor system is defined as a series of subsystems, using mathematical transfer function matrices to connect to each other the lumped acoustic elements. Usually, in these acoustic networks only one-dimensional or two-dimensional simplified configurations can be considered. In contrast with these simplified configurations, LES codes are proposed in order to investigate the whole phenomenon of combustion instability, matching pressure oscillations with turbulent combustion phenomena, even if they require large numerical resources. The finite element solution of the forced wave equation can overcome such limitations; it allows to examine three-dimensional complex geometries and to search for the complex eigenfrequencies of the system. This approach solves numerically the differential equation ruling the system, after it has been converted into a complex eigenvalue problem in the frequency (or time) domain. Complex eigenvalues of the system allow us to understand if the corresponding mode is unstable or if the oscillations will decrease in time, i.e. the mode is stable. A choice has to be made at the beginning of a thermoacoustic combustion instability analysis: a simplified analysis with simple one- or two-dimensional geometries can be carried out, possibly accounting for some important acoustic parameters, or a more complex analysis can be decided for, with a geometry very close to the real one, but with strong simplifications (i.e. the neglect of the mean flow in the system).

In this paper a quantitative comparison between a low order model, called LOMTI, and a FEM approach, which has been described and tested in previous papers, is presented. LOMTI models Ansaldo combustor as a simplified system of cylinders and annular ducts, whereas the FEM approach model this combustor with a three-dimensional geometry very close to the real one. A difference between these approaches stands in the flame models: LOMTI considers a traditional heat release law with a flat flame concentrated at the beginning of the combustion chamber, whereas the FEM approach can model heat release law both with a concentrated flame and with spatially distributed heat release. Unlike LOMTI, the FEM approach neglects some important acoustic parameters, such as mean flow, viscosity coefficient, entropy and vorticity waves. In fact, in order to overcome some of these strong assumptions, a burner transfer matrix, that is a typical low order tool, has been introduced in the FEM approach.

In order to predict the worst thermoacoustic conditions in combustion systems modelling those of Ansaldo, these two approaches are developed and a comparison is carried out. An exact agreement is very hard to reach, because of the different approximations made in each approach. The main aim of this comparison is to examine if there is the possibility to interface one method with the other, exploiting their respective good properties. In a first phase, the FEM results may be used to calibrate the geometrical dimensions of the ducts in LOMTI so that eigenfrequencies are optimally matched; in a second phase, LOMTI can be used to carry out a rapid parametric analysis, to identify optimal conditions to be used by designers.

This paper presents at the beginning a general introduction of the two different approaches. A first comparison is done on the shape of the system's eigenmodes. Then the comparison is extended to the frequencies and growth rates of the combustor when

unsteady heat release is introduced. On the basis of the results obtained the ways in which it is possible to interface LOMTI and the FEM approach are discussed.

1 MATHEMATICAL MODEL

The configuration chosen to schematize the turbine analyzed is that in Fig. 1 (left frame). It consists in an annular plenum connected to an annular combustion chamber via $N_b = 24$ identical cylindrical premixers. The geometrical parameters of the model configuration are those in Tab. 1.

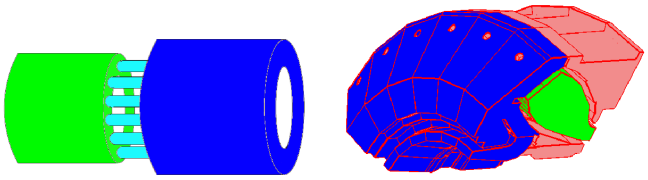

FIGURE 1. Left: general view (not to scale) of the configuration with 8 of the 24 premixers shown. Right: view of the corresponding real geometry; pink volumes are not modelled in LOMTI's approach. The plenum is in blue and the combustion chamber is in green.

(a) Plenum

length	L_1 [m]	2.3
radius	R_1 [m]	1.7
width	δ_1 [m]	0.435

(b) Premixers

length	L_2 [m]	0.142
area	A_2 [m^2]	0.034

(c) Combustion chamber

length	L_3 [m]	1.3
radius	R_3 [m]	1.55
width	δ_3 [m]	0.355

TABLE 1. Geometrical data for (a) the plenum, (b) the premixers and (c) the combustion chamber of LOMTI's model configuration.

1.1 FEM approach

The fluid is treated as an ideal gas, so that the ratio of the specific heats is considered constant. Flow velocity is regarded as negligible, except in some areas, such as the conduits of the burner, which are modelled by means of specific transfer function matrices. The effects of viscous losses and heat transfer through the walls is neglected. Under such hypotheses, in the presence of heat release fluctuations at the flame, the inhomogeneous wave equation is:

$$\frac{1}{\overline{c}^2}\frac{\partial^2 p'}{\partial t^2} - \overline{\rho}\nabla\cdot\left(\frac{1}{\overline{\rho}}\nabla p'\right) = \frac{\gamma-1}{\overline{c}^2}\frac{\partial q'}{\partial t}, \tag{1}$$

where q' is the fluctuation of the heat input per unit volume, the prime denotes a perturbation and overbars denote time average mean value. The RHS of Eq. (1) is a monopole source of acoustic pressure disturbances. Supposing the mean flow velocity negligible, no entropy nor vorticity wave is generated and the pressure fluctuations are related to the velocity fluctuations by

$$\frac{\partial \mathbf{u}'}{\partial t} + \frac{1}{\overline{\rho}}\nabla p' = 0. \tag{2}$$

Pressure and velocity fluctuations are expressed by complex functions of time and position

$$p' = \Re(\widehat{p}(\mathbf{x})\exp(i\omega t)), \qquad \mathbf{u}' = \Re(\widehat{\mathbf{u}},(\mathbf{x})\exp(i\omega t)) \tag{3}$$

where ω is the complex frequency. Its real part gives the frequency of oscillations, while the imaginary part provides the growth rate at which the amplitude of the oscillations increases per cycle. Also, the heat release fluctuation can be represented as a complex function:

$$q' = \Re(\widehat{q}(\mathbf{x})\exp(i\omega t)). \tag{4}$$

Then, using Eq. (1) and Eq. (3), the acoustic pressure waves are governed by the following equation

$$\frac{\lambda^2}{\overline{c}^2}\widehat{p} - \overline{\rho}\nabla\cdot\left(\frac{1}{\overline{\rho}}\nabla\widehat{p}\right) = -\frac{\gamma-1}{\overline{c}^2}\lambda\widehat{q} \tag{5}$$

where $\lambda = -i\omega$ and c is the speed of sound. Eq. (5) represents a quadratic eigenvalue problem which is solved by means of an iterative linearization procedure.

The mathematical model of the burners, expressed as lumped elements, is represented by a system of linear equations, which is the transfer matrix. In this system the unknown are the fluctuations of acoustic pressure p' and acoustic velocity u' at the junctions, or ports of the element. The burner can be modelled as a compact element using a transfer matrix obtained through

experimental data [9–11]. Assuming a one-dimensional flow and linearizing the mass and the conservation equations, it is obtained

$$\left[A\left(\frac{p'}{\bar{\rho}c}M+u'\right)\right]_u^d=0, \tag{6}$$

$$\frac{i\omega}{c}u'_u l_{eff}+\left[Mu'+\frac{p'}{\bar{\rho}c}\right]_u^d+\zeta M_d u'_d=0. \tag{7}$$

In Eq. (7) the effective length l_{eff} is a measure of the accelerated mass in the compact element:

$$l_{eff}=\int_{x_u}^{x_d}\frac{A_u}{A(x)}\,dx, \tag{8}$$

and it takes into account the variation of section between plenum and burner. ζ is an acoustic loss, generally related to the time mean flow loss coefficient. Using an effective length l_{eff} and a pressure loss coefficient ζ, neglecting higher order Mach number terms, the transfer matrix of a compact element is obtained from Eq. (6) and Eq. (7) as:

$$\begin{bmatrix}\frac{p'}{\bar{\rho}c}\\ u'\end{bmatrix}_d=\begin{bmatrix}1 & M_u-\alpha M_d(1+\zeta)-ikl_{eff}\\ \alpha M_u-M_d & \alpha+M_d ikl_{eff}\end{bmatrix}\begin{bmatrix}\frac{p'}{\bar{\rho}c}\\ u'\end{bmatrix}_u \tag{9}$$

where $k=\omega/c$ is the wave number and $\alpha=A_u/A_d$ is the area ratio.

1.2 LOMTI's approach

The basic idea of LOMTI (acronym of *Low Order Model for Thermoacoustic Instabilities*) is to analyze the gas turbine through a set of equations suited to represent the system. The approach chosen is a time-domain state space representation derived from modern control theory. The internal state variables are the smallest possible subset of system variables that can represent the entire state of the system at any given time. The variables are expressed as vectors and the differential and algebraic equations that represent the system are written in matrix form (the latter only being possible when the dynamical system is linear or linearized). Since LOMTI avails of a lumped approach the system is uniquely represented by the amplitude of the perturbations of the thermodynamical variables in each duct together with heat release perturbations at the flame. Equations are deduced from conservation principles at the junctions of each duct (jump conditions) and well posed boundary conditions. Furthermore a transfer function that couples heat release with other variables is required to close the problem when flame pertubations are taken into account.

Mean flow computation. A preliminary computation of the thermodynamic parameters in each duct is required. Since a lumped approach is used the unknowns are ($\bar{p}$, $\bar{T}$, $\bar{\rho}$, $\bar{u}$) in each duct along with the total heat release $\bar{q}$. They will be identified in the plenum, premixers and combustion chamber, with subscript 1, 2 and 3 respectively. Since all the premixers are identical, the mean flow parameters should be the same for each premixer. We can thus consider only one set of unknowns ($\bar{p}_2$, $\bar{T}_2$, $\bar{\rho}_2$, $\bar{u}_2$) for all the premixers, so that the total number of unknowns is 13.

The available equation are: a perfect gas equation in each duct ($\bar{p}=\bar{\rho}R\bar{T}$); the mass flux conservation, written locally at each premixer inlet or outlet ($\dot{\bar{m}}_1=N_b\cdot\dot{\bar{m}}_2=\dot{\bar{m}}_3$); the energy conservation between the plenum and the premixers ($\dot{\bar{m}}_1\bar{H}_1=N_b\cdot\dot{\bar{m}}_2\bar{H}_2$) and at the combustion chamber inlet ($\dot{\bar{m}}_3\bar{H}_3=\dot{\bar{m}}_1\bar{H}_1+A_3\bar{Q}$); the isentropic condition – usually for an area decrease – at plenum-premixers junctions ($\bar{p}_1/\bar{p}_2=(\bar{\rho}_1/\bar{\rho}_2)^\gamma$); a Borda-like equation at the premixers exit ($\dot{\bar{m}}_2\bar{u}_2-\dot{\bar{m}}_3\bar{u}_3=A_3(\bar{p}_3-\bar{p}_2)$). It is thus sufficient to have 4 input data, for instance the pressure, temperature and mass flux at the plenum inlet, along with the flame temperature, to compute all the mean flow parameters.

The input parameters chosen for the mean flow calculation are taken to be:

$$\begin{cases}\bar{p}_1 & = 17.5\text{ bar},\\ \bar{T}_1 & = 700\text{ K},\\ \bar{p}_3 & = 16.7\text{ bar},\\ T_{flame}=\bar{T}_3 & = 1730\text{ K}.\end{cases}$$

Eigenmodes computations. In the present configuration, the burners are assumed to be azimuthally and radially compact [8], which means that both their diameter and the burner-to-burner distance should be smaller than the azimuthal and radial wavelengths of all modes considered. Under this assumption, only longitudinal perturbations propagate in the burners with the form

$$\begin{aligned}p' &= \left(A^+e^{ik^+x}+A^-e^{ik^-x}\right)e^{i\omega t},\\ \rho' &= \frac{1}{\bar{c}^2}\left(A^+e^{ik^+x}+A^-e^{ik^-x}-A^e e^{ik^0x}\right)e^{i\omega t},\\ u' &= -\frac{1}{\bar{\rho}}\left(\frac{k^+}{\alpha^+}A^+e^{ik^+x}+\frac{k^-}{\alpha^-}A^-e^{ik^-x}\right)e^{i\omega t},\\ T' &= \frac{1}{c_p\bar{\rho}}\left[\left(A^+e^{ik^+x}+A^-e^{ik^-x}\right)+\frac{1}{\gamma-1}A^e e^{ik^0x}\right]e^{i\omega t},\end{aligned} \tag{10}$$

with

$$\begin{cases}k^\pm=\dfrac{M\omega\mp|\omega^2|}{\bar{c}(1-M^2)},\\ k^0=-\dfrac{\omega}{\bar{u}},\\ \alpha^\pm=\omega+\bar{u}k^\pm.\end{cases} \tag{11}$$

In the plenum and combustion chamber, the perturbation is a combination of $N_n = N_b$ (even) azimuthal modes:

$$\begin{aligned}
p' &= \sum_{n=-N_n/2+1}^{N_n/2} \left(A_n^{\pm} e^{ik^{\pm}x}\right) B_{n,m}(r)\,\Omega,\\
\rho' &= \sum_{n=-N_n/2+1}^{N_n/2} \frac{1}{\overline{c}^2}\left[\left(A_n^{\pm} e^{ik^{\pm}x}\right) B_{n,m}(r) - A_n^e e^{ik^0 x} E(r)\right]\Omega,\\
u' &= \sum_{n=-N_n/2+1}^{N_n/2} -\frac{1}{\overline{\rho}}\left(\frac{k^{\pm}}{\alpha^{\pm}} A_n^{\pm} e^{ik^{\pm}x}\right) B_{n,m}(r)\,\Omega,\\
v' &= \sum_{n=-N_n/2+1}^{N_n/2} \frac{i}{\overline{\rho}}\left(\frac{1}{\alpha^{\pm}} A_n^{\pm} e^{ik^{\pm}x}\right) \frac{dB_{n,m}(r)}{dr}\,\Omega,\\
w' &= \sum_{n=-N_n/2+1}^{N_n/2} -\frac{n}{r\overline{\rho}}\left(\frac{1}{\alpha^{\pm}} A_n^{\pm} e^{ik^{\pm}x}\right) B_{n,m}(r)\,\Omega,\\
T' &= \sum_{n=-N_n/2+1}^{N_n/2} \frac{1}{c_p\overline{\rho}}\left[\left(A_n^{\pm} e^{ik^{\pm}x}\right) B_{n,m}(r) + \frac{E(r)}{\gamma-1} A_n^e e^{ik^0 x}\right]\Omega,
\end{aligned} \tag{12}$$

where

$$\begin{cases}
k^{\pm} = k_{n,m}^{\pm} = \dfrac{M\omega \mp \sqrt{\omega^2 - \chi_{n,m}^2 \overline{c}^2 (1-M^2)}}{\overline{c}(1-M^2)},\\
k^0 = -\dfrac{\omega}{\overline{u}},\\
\alpha^{\pm} = \alpha_{n,m}^{\pm} = \omega + \overline{u} k_{n,m}^{\pm},\\
A_n^{\pm} e^{ik^{\pm}x} = A_n^{+} e^{ik^{+}x} + A_n^{-} e^{ik^{-}x},\\
\Omega = e^{i\omega t + in\theta},
\end{cases} \tag{13}$$

with n and m the azimuthal and radial wavenumbers respectively. $\chi_{n,m} \geq 0$ is defined to be the $(m+1)$th solution of $\frac{dJ_n}{dr}(\chi_{n,m}R_3) = 0$, in the chamber, and $\frac{dY_n}{dr}(\chi_{n,m}R_{1o})\frac{dJ_n}{dr}(\chi_{n,m}R_{1i}) - \frac{dJ_n}{dr}(\chi_{n,m}R_{1o})\frac{dY_n}{dr}(\chi_{n,m}R_{1i}) = 0$, in the plenum, with J_n and Y_n the Bessel functions of the first and second kind, respectively. The function $E(r)$ is arbitrary and

$$B_{n,m}(r) = \frac{dY_n}{dr}(\chi_{n,m}R_{1o})J_n(\chi_{n,m}r) - \frac{dJ_n}{dr}(\chi_{n,m}R_{1o})Y_n(\chi_{n,m}r), \tag{14}$$

in the chamber, and $B_{n,m}(r) = J_n(\chi_{n,m}r)$, in the plenum.

Note that, even if the perturbation velocity in the plenum and combustion chamber have azimuthal and radial components, they do not appear in the set of equations arising from the linearization of the mean flow system. Indeed, since only longitudinal waves propagate in the burners, there is no direct coupling of the azimuthal and radial velocity across them [8]. The components v' and w' of the velocity appear only in the energy conservation equation through the enthalpy $H' = (c_pT + (u^2+v^2+w^2)/2))'$ as terms which vanish. Nonetheless, the expression of v' and w' could be recovered from the equations above, once the computation is completed.

Under the hypothesis that flames issuing from neighboring injectors do not interact, we use the so-called ISAAC (*Independence Sector Assumption in Annular Combustor*) assumption [12] to define the flame transfer function. It states that

> "the heat release fluctuations in a given sector [of the combustion chamber] are only driven by the fluctuating mass flow rates due to the velocity perturbations through its own swirler."

This means that a local transfer function is written for each of the N_b flames with a specific perturbation in heat release $(Q_j)'$, $1 \leq j \leq N_b$, and with a different reference point each time, chosen at the inlet of every premixer:

$$\frac{(Q_j)'}{\bar{Q}} = \kappa_j \frac{u_j'}{\bar{u}_j} e^{-i\omega\tau_j}$$

In this specific case we deal with identical premixers, thus $\kappa_j = \kappa$ and $\tau_j = \tau$ for all flame transfer functions. Different kinds of inlet and outlet conditions are implemented in LOMTI. In this paper, only closed-end inlet and outlet conditions are used, for codes comparison purpose.

2 RESULTS

2.1 Annular Combustion Chamber Modes

The geometry chosen to represent the combustors used by Ansaldo Energia has been modelled in three dimensions. Following an approach tested in other works [13–15], only a quarter of the whole combustor has been analyzed, applying symmetry conditions on periodic faces. The scheme is plotted in Fig. 1.

Transfer matrix has been applied removing every burner, so that the upstream port of each matrix is the exit from the plenum and the downstream is the inlet of the combustion chamber, following the criteria discussed in [15]. Operating conditions can be taken from experimental data or from RANS simulations of combustion [16]. In Fig. 2 an example of the temperature field inside the combustor is shown.

Importing in the FEM code the temperature field from a RANS simulation, it is possible to solve the eigenvalue problem with the actual temperatures inside the combustion chamber, defining as well as possible the flame shape. Doing so, the flame is not considered any more as a flame sheet or as a thin domain with a uniform temperature, but it has a realistic shape.

From Fig. 3 to Fig. 12 the comparison between the neutral modes obtained in LOMTI and the corresponding ones obtained with the FEM analysis is shown, for the case in which the mean flow is neglected and there are no heat release fluctuations at the

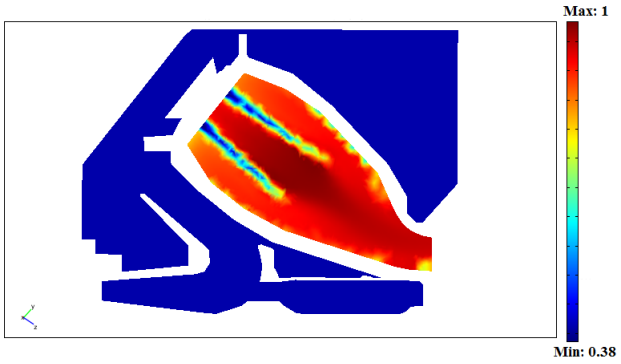

FIGURE 2. Temperature field from RANS simulation.

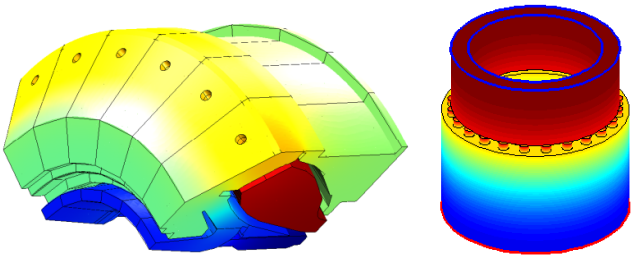

FIGURE 3. Mode 3, purely axial waveform. Normalized frequency from FEM analysis: $f_{FEM} = 1.35$. Frequency from LOMTI with same normalization: $f_{LOMTI} = 1.31$.

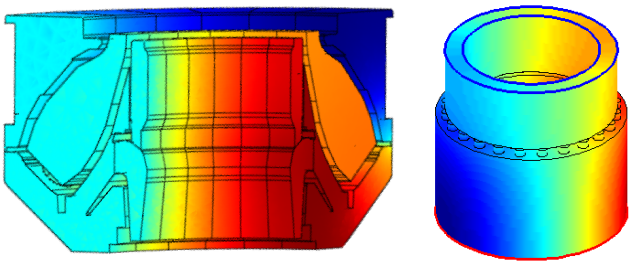

FIGURE 4. Mode 4, azimuthal wavenumber $n = 1$. Normalized frequency from FEM analysis: $f_{FEM} = 1.65$. Frequency from LOMTI with same normalization: $f_{LOMTI} = 1.05$.

flame. The frequencies are normalized by the lowest eigenfrequency found in the FEM approach.

As it can be seen from these figures, there is a very good agreement between the low-order model and the finite element simulation. All in all, 11 of the 16 neutral modes obtained with the FEM software have been reproduced with LOMTI, at frequencies close to those obtained with the more complex tool. This means that 5 of the FEM modes have not been detected.

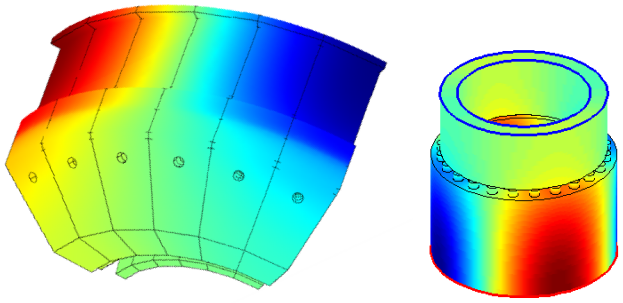

FIGURE 5. Mode 5, azimuthal wavenumber $n = 2$. Normalized frequency from FEM analysis: $f_{FEM} = 1.97$. Frequency from LOMTI with same normalization: $f_{LOMTI} = 1.97$.

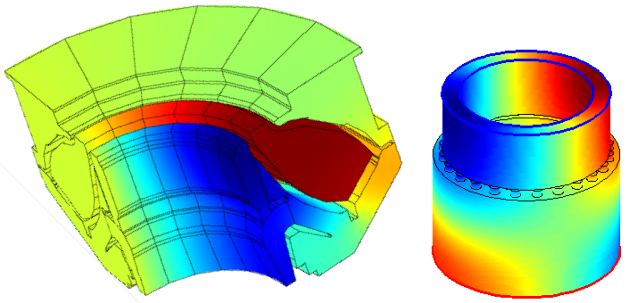

FIGURE 6. Mode 6, azimuthal wavenumber $n = 1$. Normalized frequency from FEM analysis: $f_{FEM} = 2.17$. Frequency from LOMTI with same normalization: $f_{LOMTI} = 1.91$.

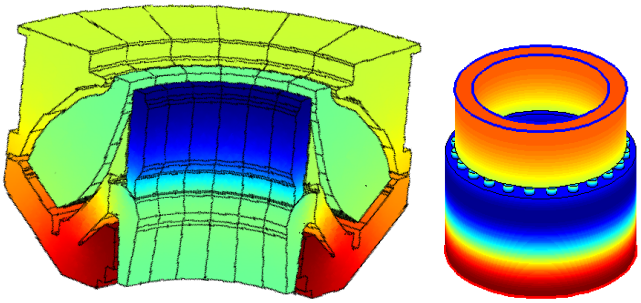

FIGURE 7. Mode 7, purely axial waveform. Normalized frequency from FEM analysis: $f_{FEM} = 2.34$. Frequency from LOMTI with same normalization: $f_{LOMTI} = 2.60$.

Examining three of these modes, it is clear why LOMTI has not detected them: these modes are confined in a very small corner of the plenum (pink volumes in Fig. 1), at a very small length-scale, so they could not - and should not - have a corresponding mode in the lumped parameter approximation. Considering their location in the plenum, they are anyway very unlikely to yield humming. It is less clear why the other 2 modes (not shown)

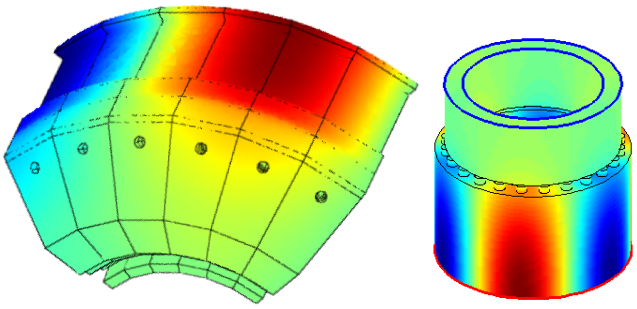

FIGURE 8. Mode 8, azimuthal wavenumber $n = 3$. Normalized frequency from FEM analysis: $f_{FEM} = 2.82$. Frequency from LOMTI with same normalization: $f_{LOMTI} = 2.85$.

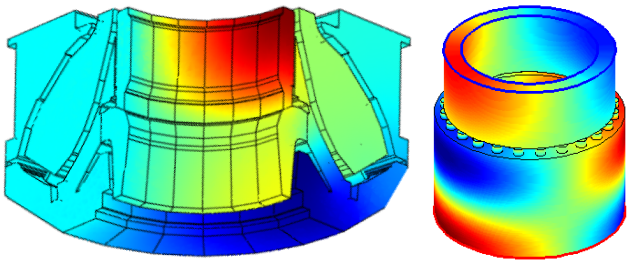

FIGURE 9. Mode 9, azimuthal wavenumber $n = 1$. Normalized frequency from FEM analysis: $f_{FEM} = 2.81$. Frequency from LOMTI with same normalization: $f_{LOMTI} = 2.81$.

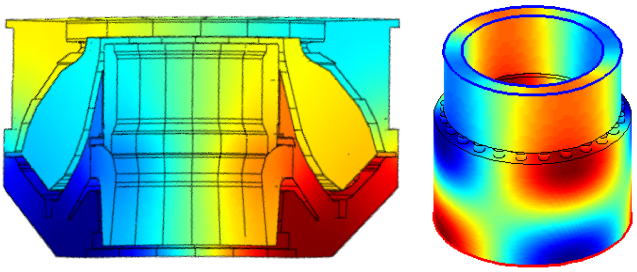

FIGURE 10. Mode 10, azimuthal wavenumber $n = 2$. Normalized frequency from FEM analysis: $f_{FEM} = 2.81$. Frequency from LOMTI with same normalization: $f_{LOMTI} = 2.92$.

have not been identified. These two modes are plenum modes and there is no obvious reason why they should not be found by LOMTI when the other plenum modes are. A possible solution could be to model the plenum in LOMTI into several ducts of different diameter, in the hope that these modes would thus emerge. It is very significant, nonetheless, that all the combustion chamber modes have been identified by the low order model, as shown in the figures.

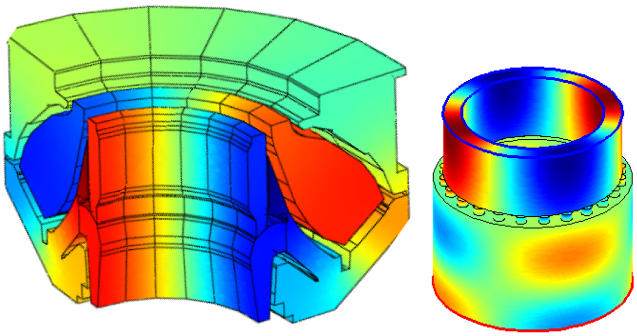

FIGURE 11. Mode 13, azimuthal wavenumber $n = 2$. Normalized frequency from FEM analysis: $f_{FEM} = 3.61$. Frequency from LOMTI with same normalization: $f_{LOMTI} = 3.57$.

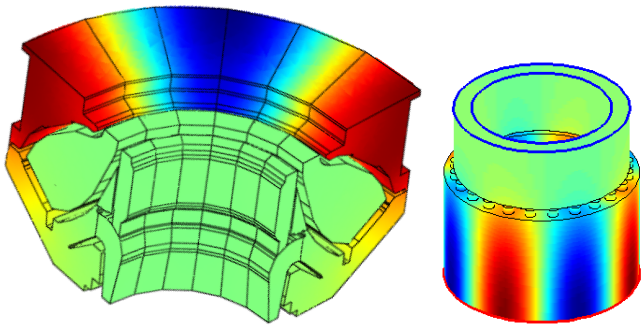

FIGURE 12. Mode 14, azimuthal wavenumber $n = 4$. Normalized frequency from FEM analysis: $f_{FEM} = 3.67$. Frequency from LOMTI with same normalization: $f_{LOMTI} = 3.74$.

2.2 Annular Combustion Chamber with Heat Release Fluctuations

After the preliminary comparison of the previous section we are able to perform a further comparison with a switched on flame with reasonable confidence. Again we have to set the same boundary conditions and operating parameters between the two approaches. Moreover the same flame transfer function should be used in order to compare results. Differing from the usual approach the reference point to compute τ for the equation below is now chosen at the beginning of the combustion chamber. This does not imply that the reference is placed right on the flame, because in FEM the flame is not modelled as a flat sheet but it is a three-dimensional surface evolving into the combustion chamber.

Since the temperature field is not uniform in each component, it is possible to model a three dimensional flame front with FEM as shown in Fig. 2 and in Fig. 13, where the reaction rate from a RANS simulation is shown. Heat release is defined from

the model:

$$\frac{\widehat{q}}{\overline{q}}(\mathbf{x}) = -\kappa \frac{\widehat{u}_i}{\overline{u}_i} \exp(-j\omega\tau(\mathbf{x})), \tag{15}$$

where q is the volumetric heat release rate, $\overline{q}$ is its mean value, $\widehat{q}$ is its complex value. Subscript i corresponds to the acoustic velocity fluctuation reference position, at the beginning of the combustion chamber. In this case it is assumed that:

$$\overline{q} = RR(\mathbf{x}) \cdot LHV \cdot MM \tag{16}$$

where $RR(\mathbf{x})$ is the *Rate of Reaction*, LHV is the Lower Heating Value, MM is the Molecular Mass. Using Eq. (16) and Eq. (5) heat release law to be located within the computational domain of the combustion chamber computational domain is obtained. The time delay τ is taken constant in the two approaches (rather than a function of the oscillation frequency), and we have chosen $\tau = 7ms$.

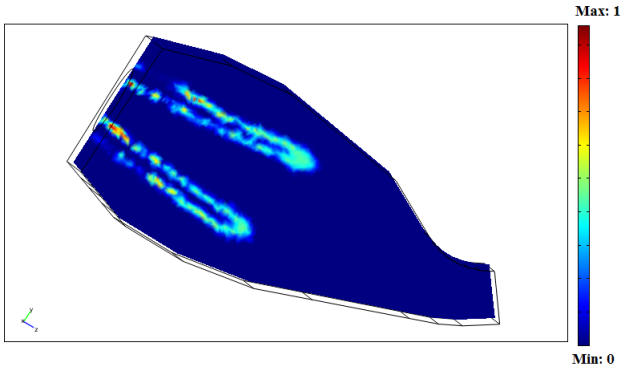

FIGURE 13. Reaction Rate from RANS simulation.

TABLE 2. Comparison between LOMTI and FEM. The last column assesses, in one word, the quality of agreement achieved. Frequency is normalized against the first eigenfrequency. Growth rate is [Hz].

Number	FEM	LOMTI	Agreement
1	1.00 - 4.65i	-	undetected
2	1.10 - 5.21i	-	undetected
3	1.47 - 45.85i	1.01 + 129.1i	bad
4	1.69 + 3.48i	0.92 - 25.9i	bad
5	1.93 - 3.70i	1.94 + 24.4i	good
6	2.09 + 1.34i	2.68 - 4.0i	bad
7	2.30 - 14.85i	2.25 - 4.3i	good
8	2.78 - 1.70i	2.83 - 2.2i	good
9	2.77 - 16.64i	2.86 - 4.3i	good
10	2.85 - 4.75i	3.10 - 0.01i	good
11	3.11 - 3.13i	-	undetected
12	3.54 - 2.19i	-	undetected
13	3.60 - 38.04i	3.54 - 39.6i	good
14	3.62 - 1.03i	3.80 - 19.0i	good
15	3.82 - 6.96i	3.54 + 89.9i	bad
16	3.89 - 1.00i	-	undetected

We have just argued that the FEM approach is very different from LOMTI's. Even though the flame obtained from a RANS simulation is not completely reliable, since the details of the turbulent field affect significantly the reaction rate, the difference from the thin flat flame used in LOMTI and the spatially distribuited temperature field used in the FEM model is evident.

In Tab. 2 the results found by LOMTI and the FEM software are summarized, together with a one-word assessment that refers to how well frequency and growth rate match for each mode. The frequency is normalized by the lowest value found in the FEM approach.

In Fig. 14 the comparison between the eigenmodes identified with LOMTI and with the FEM approach is shown. The agreement can be deemed satisfactory, considering the differences in the two techniques and, in particular, the different flames in the two cases. Mode 3 and Mode 15 are located in the plenum and for these two modes there is the greater difference between the adopted approaches. Mode 4 and Mode 6, for which there is a significant difference in the frequency value, are located both in the plenum and in the combustion chamber. Other modes exhibit little differences in the frequency or growth rate values and some modes exhibit a very good agreement.

Considering the strong geometric approximations used in LOMTI, the matching of LOMTI results with FEM's is very good, both with and without flame fluctuations and the capacity of LOMTI's simple model to obtain analogous results with a much smaller computational time is doubtless satisfying. In particular, there is a very good agreement between the two ap-

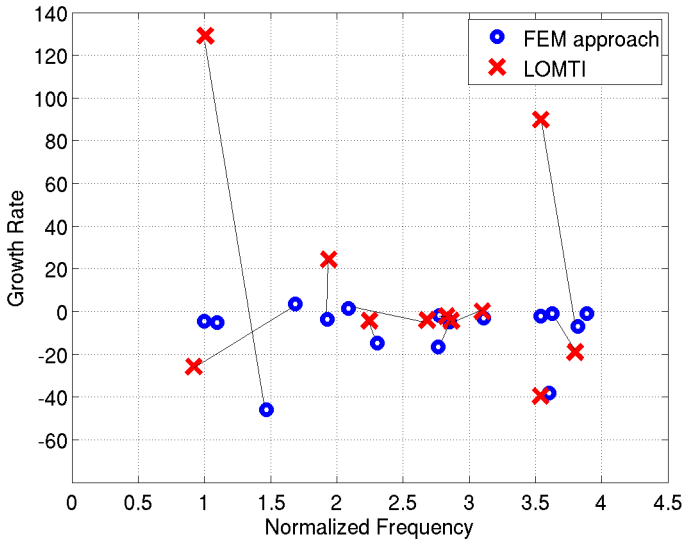

FIGURE 14. Comparison between FEM (blue circles) and LOMTI (red crosses) when heat release fluctuations are considered.

proaches in relation to the modes which are suspected from experiments to yield humming.

3 CONCLUSIONS

A comparison between a low order model, called LOMTI, and three-dimensional finite element computations has been done, for an academic model of a gas turbine. LOMTI supports only simplified geometries composed of a network of cylindrical and annular ducts, so that a matching analysis needs to be done to select the appropriate ducts' dimensions in LOMTI to reproduce as accurately as possible the real combustor. The three-dimensional FEM approach models Ansaldo combustor with its realistic geometry with the actual temperature field inside the combustion chamber, such as the actual flame shape, exploiting data coming from RANS simulations.

After having described the two different approaches, the acoustic modes have been detected both with LOMTI and the FEM analysis. All in all, comparing the obtained values, an appreciably good agreement results both with and without unsteady heat release, considering the approximations of the two approaches. Without heat release fluctuations, all the interesting modes are detected by LOMTI, which does not capture only 5 plenum modes, mainly confined in a corner of the domain. It is very important that all the combustion chamber modes are present in LOMTI's computations, above all those modes suspected to yield humming.

More differences arise when unsteady heat release is introduced into the system. These are due to the different flame models considered in the two approaches. LOMTI adopts a traditional heat release law, with a flat flame front, whereas in the FEM approach RANS simulations provide the useful information for flame shape and heat release law.

A possible advantage of LOMTI, at present, lies in its ability to easily include a mean flow, to assess the influence of entropy and vorticity waves. As a general rule, low order models can be used to carry out parametric analyses, which may be exploited later by FEM codes to investigate in more details optimized shapes. FEM code can be used to carry out the modal analyses on a three dimensional domain very close to the real one, so that the obtained results may be useful for the calibration of the simplified low order models geometries. The two approaches together provide information of value to the designers, and of possible use during online operations.

ACKNOWLEDGMENT

Support for the work over the years comes from Ansaldo Energia, and is gratefully acknowledged.

REFERENCES

[1] Akamatsu, S., and Dowling, A. "Three dimensional thermoacoustic oscillation in a premix combustor". *ASME paper 2001-GT-0034*.

[2] Bellucci, V., Schuermans, B., Novak, D., Flohr, P., and Paschereit, C., 2005. "Thermoacoustic modeling of a gas turbine combustor equipped with acoustic dampers". *Journal of Turbomachinery,* ***127***(2), pp. 372–379.

[3] Schuermans, B., Bellucci, V., Guethe, F., Meili, F., Flohr, P., and Paschereit, C. "A detailed analysis of thermoacoustic interaction mechanisms in a turbulent premixed flame". *ASME paper GT2004-53831*.

[4] Martin, C., Benoit, L., Nicoud, F., and Poinsot, T. "Analysis of acoustic energy and modes in a turbulent swirled combustor". *CTR Proceedings, 2004, 377–394*.

[5] Nicoud, F., Benoit, L., Sensiau, C., and Poinsot, T., 2007. "Acoustic modes in combustors with complex impedances and multidimensional active flames". *AIAA Journal,* ***45***(2), pp. 426–441.

[6] Camporeale, S., Fortunato, B., and Campa, G., 2011. "A finite element method for three-dimensional analysis of thermoacoustic combustion instability". *Journal of Engineering for Gas Turbine and Power,* ***133***(1), p. 011506.

[7] Pankiewitz, C., and Sattelmayer, T. "Time domain simulation of combustion instability". *ASME paper, GT-2002-30063*.

[8] Evesque, S., and Polifke, W., 2002. "Low-order acoustic modelling for annular combustors: validation and inclusion of modal coupling". *ASME paper GT2002-30064*.

[9] Polifke, W. “Combustion instabilities”. *von Kármán Institute Lecture Series, March 2004*.

[10] Polifke, W., Paschereit, C., and Doebbeling, K., 2001. “Constructive and destructive interference of acoustic and entropy waves in a premixed combustor with a choked end”. *Int. J. of Acoustics and Vibration,* ***6***(3), pp. 1–12.

[11] Schuermans, B., 2003. “Modelling and control of thermoacoustic instabilities”. PhD Thesis, École Poytechnique Fédérale de Lausanne.

[12] Sensiau, C., Nicoud, F., and Poinsot, T., 2008. “Thermoacoustic analysis of an helicopter combustion chamber”. *AIAA paper AIAA-2008-2947*.

[13] Waltz, G., Krebs, W., Hoffmann, S., and Judith, H., 2002. “Detailed analysis of the acoustic mode shapes of an annular combustion chamber”. *J. Eng. Gas Turbines and Power,* ***124***(1), pp. 3–9.

[14] Forte, A., Camporeale, S., Fortunato, B., Bisceglie, F. D., and Mastrovito, M. “Effect of burner and resonator impedances on the acoustic behaviour of annular combustion chamber”. *ASME paper, GT-2006-90423*.

[15] Campa, G., and Camporeale, S. “Influence of flame and burner transfer matrix on thermoacoustic combustion instability modes and frequencies”. *ASME paper, GT2010-23104*.

[16] Zito, D., Bonzani, F., Piana, C., and Chiarioni, A. “Design validation on pressurized test rig of upgraded velonox^{TM}combustion system for f-class engine”. *ASME paper, GT2010-22256*.